Journal of
**Applied Crystallography**
ISSN 0021-8898

Received 2 December 2004
Accepted 3 October 2005

# Screening and optimization of protein crystallization conditions through gradual evaporation using a novel crystallization platform

**Sameer Talreja,[a] David Y. Kim,[b] Amir Y. Mirarefi,[c] Charles F. Zukoski[a,c] and Paul J. A. Kenis[a,d]***

[a]Department of Chemical & Biomolecular Engineering, University of Illinois at Urbana-Champaign, Urbana, IL 61801, USA, [b]Department of Chemical and Biological Engineering, Northwestern University, Evanston, IL 60208, USA, [c]Center for Biophysics and Computational Biology, University of Illinois at Urbana-Champaign, Urbana, IL 61801, USA, and [d]Institute for Genomic Biology and Beckman Institute, University of Illinois at Urbana-Champaign, Urbana, IL 61801, USA. Correspondence e-mail: kenis@uiuc.edu, czukoski@uiuc.edu

High-throughput screening of a wide range of different conditions is typically required to obtain X-ray quality crystals of proteins for structure–function studies. The outcomes of individual experiments, *i.e.* the formation of gels, precipitates, microcrystals, or crystals, guide the search for and optimization of conditions resulting in X-ray diffraction quality crystals. Unfortunately, the protein will remain soluble in a large fraction of the experiments. In this paper, an evaporation-based crystallization platform is reported in which droplets containing protein and precipitant are gradually concentrated through evaporation of solvent until the solvent is completely evaporated. A phase transition is thus ensured for each individual crystallization compartment; hence the number of experiments and the amount of precious protein needed to identify suitable crystallization conditions is reduced. The evaporation-based method also allows for rapid screening of different rates of supersaturation, a parameter known to be important for optimization of crystal growth and quality. The successful implementation of this evaporation-based crystallization platform for identification and especially optimization of crystallization conditions is demonstrated using the model proteins of lysozyme and thaumatin.



## 1. Introduction

A detailed understanding of the protein structure–function relationships is important in elucidating complex biochemical pathways (McPherson, 1999; Kanelis *et al.*, 2001; Thuman-Commike, 2001). The link between structure and function of a protein is usually derived by obtaining the three-dimensional structure of the protein *via* X-ray crystallography, NMR, or other means (Hornak, 1999; McPherson, 1999). Structure determination using X-ray crystallography is often hindered by the difficulties in obtaining high-quality protein crystals (McPherson, 1999). These difficulties can be attributed to the inadequate understanding of the kinetics of protein crystal nucleation and growth processes (Anderson & Lekkerkerker, 2002). No methods exist to predict *a priori* the conditions that are favorable for crystal formation. Generally, high-throughput screening methods are used to locate these conditions. Even with the use of high-throughput methods, locating optimal crystallization conditions can be a daunting task. In this paper we describe a method that provides an opportunity for rapid identification of solution conditions conducive to crystallization.

Crystallization of proteins is generally carried out by mixing a protein-containing solution with a solution containing buffers, salts and/or additives. Crystals will only form if the protein concentration is increased above its solubility to a sufficient extent; that is, if a sufficiently high level of supersaturation is reached. The driving force for the protein-containing solution to exceed the solubility boundary in commonly used crystallization screening platforms such as microbatch (MB), free interface diffusion (FID) and hanging drop (HD) differs from platform to platform (Table 1). These platforms also proceed through different paths of supersaturation toward an equilibrium condition (McPherson, 1999). Fig. 1 shows these supersaturation profiles starting from an arbitrary initial condition resembling the situation of an initially unknown solubility boundary for a novel protein. In the MB method, the equilibrium condition is reached almost instantaneously by mixing the precipitant and the protein solutions under oil. In the FID method, reservoirs containing precipitant and protein solutions are brought into contact, allowing slow counter diffusion of the precipitant and the protein. The rate of increase in supersaturation is fast in the beginning, and then slows down asymptotically over time

**Table 1**
Comparison of characteristics of different crystallization platforms.

| Description | Microbatch (MB) (McPherson, 1999) | Hanging drop (HD) (McPherson, 1999) | Free interface diffusion (FID) (McPherson, 1999) | Evaporation-based platform (this work) |
|---|---|---|---|---|
| Environment | Closed (under oil) | Closed (sealed well) | Closed (sealed in capillary) | Open (open well) |
| Driving force to exceed solubility boundary | None | Decreasing mass transfer of solvent from drop to reservoir until equal chemical potential (vapor diffusion) | Decreasing mass transfer between protein and precipitant (counter diffusion) | Constant mass transfer of solvent between the drop and (dry) air (vapor diffusion) |
| Adjustable parameters† | None | Volume of the reservoir | Length of the capillary | Area/length ratio of diffusion channel |
| Typical duration | Undefined | Undefined | Undefined | 24–72 h |
| Guaranteed phase transition | No | No | No | Yes |

† Parameters other than initial conditions (temperature, pressure, protein and precipitant concentration, and volume of the drop).

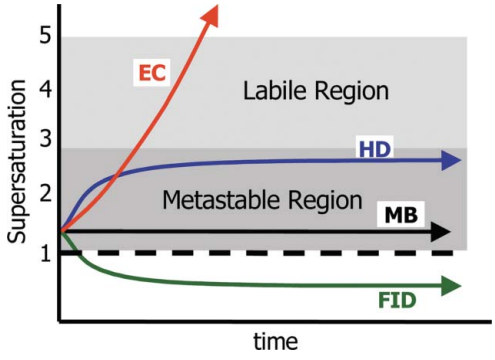


**Figure 1**
Comparison of paths through different levels of supersaturation for existing crystallization platforms (HD, FID and MB) as well as for the here-described platform (EC), starting from an arbitrary set of initial conditions. Note that in the existing platforms (HD, FID, MB) supersaturation reaches a certain equilibrium condition with time, whereas in our device (EC) the path leads through many levels of supersaturation until the endpoint of a desiccated drop is reached. Along this path phase transitions are ensured.

(Fig. 1). In the HD method, equilibrium is reached through vapor diffusion with solvent transferring out of the protein- and precipitant-containing drop into a nearby reservoir containing a higher concentration of the precipitant until the solvent in the drop and the solvent in the reservoir have the same chemical potential. The rate of evaporation, and thus the rate of increase in supersaturation, is fast at first, and then slows down while asymptotically approaching an equilibrium condition (Fig. 1). Many variations to the HD method have been developed to achieve different rates of equilibration. For example, well plates with different well or reservoir volumes, and 96-well protein crystallization microplates that facilitate screening of multiple initial conditions per well (so-called Greiner plates), are available. In the latter, each well has an elevated platform that can accommodate up to three individual sitting droplets. In addition, Collingsworth *et al.* have shown that the equilibrium condition of a drop hanging in a closed chamber can be manipulated by periodic venting of vapor phase in an HD compartment (Collingsworth *et al.*, 2000).

More recent technological developments have focused on the miniaturization of the crystallization platforms to increase the throughput and/or to reduce the amount of precious sample needed per experiment. For example, Hansen *et al.* have recently developed a rapid parallel screening system that uses the FID technique and integrated microfluidic networks (Hansen *et al.*, 2002). They explored about 144 different conditions of protein and precipitant solutions simultaneously. These microfluidic FID experiments can actually screen a broad parameter space of local protein and precipitant concentrations if the chip is continuously monitored for crystal nucleation and growth events. Ismagilov and coworkers have reported a method of rapid screening by generating several drops separated by immiscible fluids inside a microfluidic channel with each crystallizing drop screening a different set of solution conditions (Zheng *et al.*, 2003).

While the above-mentioned methods have been useful in identifying crystal-producing solution conditions, they do not ensure a phase transition or 'hit' in every experiment. Typically, the hit rates are low, thus requiring many experiments and large amounts of the often-precious protein (Hansen *et al.*, 2002). Even if the equilibrium phase behavior (*i.e.* the solubility boundary) for the protein is known or can be predicted by measuring the strength of protein–protein interactions (Rosenbaum & Zukoski, 1996), crystals may not be observed in a supersaturated solution within a reasonable period of time. This observation suggests that not only reaching a supersaturation but also the rate at which the supersaturation is reached may be the key to a successful crystallization screening method. Chayen demonstrated the importance of the rate of supersaturation by reducing the rate of vapor diffusion from a hanging drop by applying a layer of oil over the reservoir, which resulted in few large crystals (Chayen, 1997*a*,*b*).

In this paper, we report on an evaporation-based crystallization platform with enhanced capabilities: a phase transition is guaranteed in every experiment within a few days, and different rates of supersaturation can be screened easily. Furthermore, multiple conditions can be tested per screening experiment and the results of all the observed phase transitions, including the non-crystalline ones, are used to narrow down the search space for suitable crystallization conditions. Initial concentrations in the protein-containing droplet and the rate of evaporation turn out to play key roles in determining the type of the solid formed.

In §2 we discuss the design, concept and fabrication of the evaporation-based crystallization platform studied. In §3 we report a two-step protocol to identify suitable crystallization conditions for high-quality crystals with our platform using the model protein systems of hen egg white lysozyme from *Gallus gallus* and thaumatin from *Thaumatococcus daniellii*. In §4 we further analyze and discuss our observations, and in §5 we draw conclusions.

## 2. Evaporation-based crystallization platform

The crystallization platform studied here is based on the concept of regulated evaporation where the solvent from a drop in a compartment evaporates to the outside environment through a channel of predefined geometry with cross-sectional area $A$ and length $L$, as shown in Fig. 2. Gradual evaporation of solvent at a known rate set by the dimensions of the channel will drive the solution of the drop to a level of supersaturation where a phase transition is forced to occur. Since the final state will always be a completely desiccated drop, a phase transition is observed in every experiment. Assuming that the rate of evaporation is controlled by diffusion through the capillary channel, the evaporation rate $J$, the rate of volumetric loss of the solvent (at steady state), can be expressed by the equation (Geankoplis, 1993)

$$J = K(\Delta P)(A/L) \quad (1)$$

where $K$ is the overall mass transfer coefficient, $\Delta P$ is the pressure difference between the vapor phase around the drop and the outside environment, and $A$ and $L$ are the dimensions of the diffusion channel as defined above. The vapor pressure around the drop is only a weak function of the precipitant and the protein concentration until the drop is very close to complete drying. As a result, $\Delta P$ is nearly constant throughout the course of an experiment provided that the vapor pressure in the outside environment does not change appreciably. From equation (1) it follows that $J$ is nearly constant throughout the course of an experiment and only depends on the geometric ratio $(A/L)$. Experiments are designed to screen a range of rate of supersaturation generation by varying (i) the initial conditions through adjusting the initial protein and precipitant concentrations or the volume of the drop, and/or (ii) the ratio $A/L$, which allows for independent regulation of $J$.

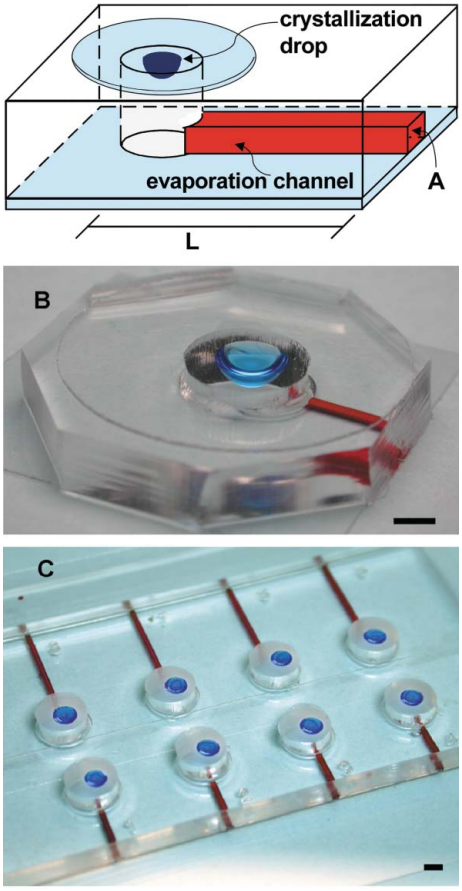


**Figure 2**
(A) Schematic of the platform: a compartment with a drop containing protein and precipitant, connected to the atmosphere through an evaporation channel of length $L$ and cross-sectional area $A$. (B) Optical micrograph of the platform: red and blue ink is used to visualize the channel and the drop, respectively. (C) Optical micrograph of multiple wells cast in a single polymer slab. Scale bar: 2 mm

### 2.1. Platform fabrication

The platform was fabricated using a rapid prototyping method (Duffy *et al.*, 1998). The master of the diffusion channel was obtained *via* photolithography using 5080 d.p.i. transparency masks and SU-8-100 positive-relief photoresist (Microchem) on 3″ silicon wafers (Wafer World). PDMS elastomer (Sylgard 184, Dow Corning) was used to obtain ∼7 mm thick replicas of the master: a PDMS mold with the diffusion channel in negative relief. A 5 mm through-hole was punched for the evaporation chamber at one end of the diffusion channel and a microscope cover slip was placed over the side of the PDMS mold with the diffusion channel. Typical dimensions used are: $L$ 5–10 mm; $A$ 250 × 250 to 1000 × 1000 µm; $A/L$ ratios 200–12.5 µm.

### 2.2. Protein and precipitant solutions

Hen egg white lysozyme protein (Seikagaku America) was dissolved in 50 m$M$ sodium acetate buffer at pH 4.6 to obtain a protein stock solution of concentration ($C_p$) 30 mg ml$^{-1}$. The concentration of the stock lysozyme solution was measured by UV–visual Spectroscopy (Hewlett-Packard 8453 UV–Vis Spectrophotometer) using an extinction coefficient of 2.64 ml mg$^{-1}$ cm$^{-1}$ at 280 nm (Sophianopoulos *et al.*, 1962). Lower-$C_p$ solutions were obtained by further dilution of the protein stock solution with buffer. A precipitant solution (2 mol l$^{-1}$ ionic strength) was prepared by adding NaCl (Sigma) to 50 m$M$ acetate buffer. Thaumatin from *Thaumatococcus daniellii* (Sigma) was dissolved in 50 m$M$ phosphate buffer at pH 7.0 to obtain a protein stock solution of concentration ($C_p$) 30 mg ml$^{-1}$. A precipitant solution (2 mol l$^{-1}$ ionic strength) was prepared by adding sodium potassium tartrate (Fisher) to 50 m$M$ acetate buffer.

For both proteins, a solution with $C_p$ = 15 mg ml$^{-1}$ and a 1 $M$ salt concentration was obtained by mixing of the

respective salt and protein stock solutions. Solutions with lower initial lysozyme or thaumatin concentration ($C_{po}$), but the same $C_p/C_s$ were obtained by dilution with acetate or phosphate buffer, respectively. Prior to use, all salt, lysozyme and thaumatin solutions were filtered through 0.02 µm (Anotop 25) or 0.2 µm (Anotop 10) pore-size filters.

### 2.3. Setup of crystallization experiments

10 µl (lysozyme) or 5 µl (thaumatin) drops of protein–precipitant mixture were pipetted on a siliconized glass slide (Hampton Research) and the glass slide was sealed to the open side of the platform with the drop(s) positioned in the evaporation chamber(s). The evaporation was carried out at ambient conditions and the drops were monitored periodically for a phase transition using an optical microscope. Phase transitions typically occurred between 24 and 120 h depending on the evaporation rate set by the $A/L$ ratio. Each experiment was repeated five times to confirm the qualitative outcomes: many small crystals; few large crystals; film; gel; amorphous precipitate or combinations of these. Optical micrographs were obtained using a stereozoom microscope (Leica MZ-12) with a CCD camera (Sony DXC-390).

Calibration of the evaporation rates was carried out by measuring the time for complete evaporation of pure water drops of various volumes. This drying time was found to vary linearly with initial drop volume. In addition, the drying times of pure water and those for drops containing salt and protein were compared. These drying times were observed to be the same, indicating that the decrease in water activity at the end of the drying process has negligible effect on the overall drying time.

## 3. Screening protocol and experiments

A two-step process is used to identify suitable conditions for protein crystallization.

Step 1: identify crystal-producing conditions by varying the initial protein ($C_p$) and precipitant ($C_s$) concentrations at a constant evaporation rate $J$.

Step 2: optimize crystal growth and quality by varying $J$ at constant $C_p$ and $C_s$.

### 3.1. Step 1: identifying crystal-producing conditions

In step 1, we hold $C_p/C_s$ constant but vary $C_p$ such that even with different initial conditions, once the drop is supersaturated, each drop traverses the same set of compositions with time. The difference between the drops is that the one with smaller initial $C_p$ will have a smaller volume once the solubility boundary is reached. At a constant rate of evaporation, this results in a faster rate of increase in $C_p$. Since each experiment traverses the same sequence of compositions, we would expect to observe essentially the same number and size of crystals in each experiment if crystal nucleation and growth were solely dependent on the composition. As discussed below, we find that the rate of increase in protein and precipitant concentration is important in determining the state of the protein in the drop.

Experiments with lysozyme were performed using sodium acetate buffer (50 m$M$, pH 4.6) with sodium chloride (NaCl) as the precipitant. In step 1, in a set of seven drops with different initial conditions but at a constant $J$ of 0.42 µl h$^{-1}$ and a constant $C_p/C_s$ of 30 g mol$^{-1}$, crystals are observed in the most concentrated drop (Fig. 3A; $C_p$ = 15 mg ml$^{-1}$, $C_s$ = 0.5 mol l$^{-1}$), whereas only a few small crystals and the formation of a film on the surface of the drop are observed at lower initial concentrations (Fig. 3B; $C_p$ = 7.5 mg ml$^{-1}$, $C_s$ = 0.25 mol l$^{-1}$). For the lowest protein concentration, only a film is produced (Fig. 3C; $C_p$ = 3.75 mg ml$^{-1}$, $C_s$ = 0.125 mol l$^{-1}$).

Similar observations are made in step 1 for thaumatin dissolved in phosphate buffer (50 m$M$, pH 7.0) with sodium potassium tartrate as the precipitant (Figs. 3F–3H). Seven different initial conditions were screened for each $C_p/C_s$ ratio of 10, 30, 50 and 100 g mol$^{-1}$ at a constant $J$ of 0.11 µl h$^{-1}$. The $C_p/C_s$ ratios of 10–50 g mol$^{-1}$ produced unfavorable phase transitions such as aggregates or films. For a $C_p/C_s$ ratio of

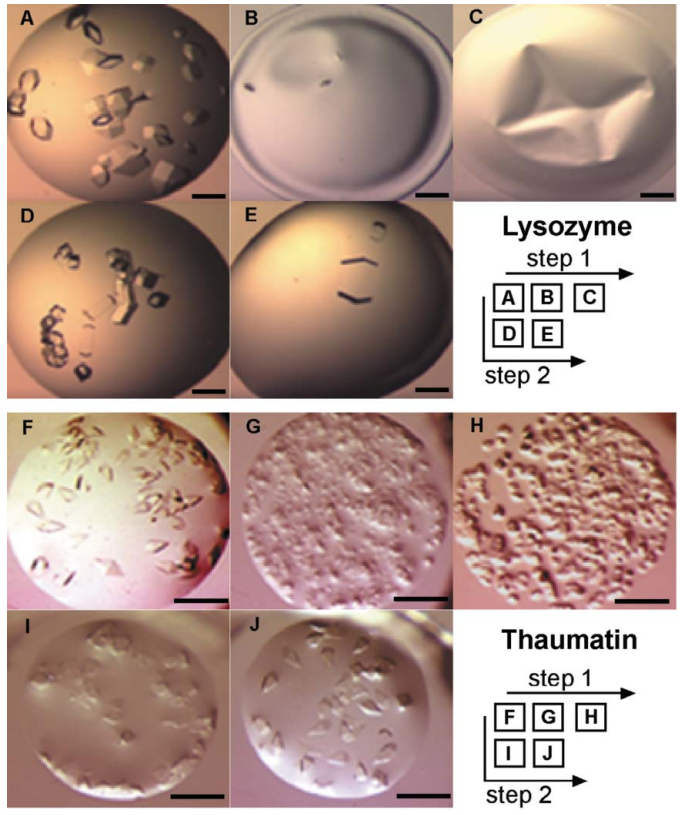


**Figure 3**
Optical micrographs of typical results obtained with the platform for different initial conditions ($C_p$, $C_s$) and evaporation rates ($J$). For lysozyme: (A) $C_p$ = 15 mg ml$^{-1}$, $C_s$ = 0.5 mol l$^{-1}$; $J$ = 0.42 µl h$^{-1}$. (B) 7.5 mg ml$^{-1}$, 0.25 mol l$^{-1}$; 0.42 µl h$^{-1}$ (~22 h). (C) 3.25 mg ml$^{-1}$, 0.125 mol l$^{-1}$; 0.42 µl h$^{-1}$ (~20 h). (D) 15 mg ml$^{-1}$, 0.5 mol l$^{-1}$; 0.11 µl h$^{-1}$ (~2 d). (E) 15 mg ml$^{-1}$, 0.5 mol l$^{-1}$; 0.026 µl h$^{-1}$ (~5 d). For thaumatin: (F) $C_p$ = 15 mg ml$^{-1}$, $C_s$ = 0.15 mol l$^{-1}$; $J$ = 0.11 µl h$^{-1}$ (~2 d). (G) 10 mg ml$^{-1}$, 0.1 mol l$^{-1}$; 0.11 µl h$^{-1}$ (~3 d). (H) 5 mg ml$^{-1}$, 0.05 mol l$^{-1}$; 0.11 µl h$^{-1}$ (~3 d). (I) 15 mg ml$^{-1}$, 0.15 mol l$^{-1}$; 0.0275 µl h$^{-1}$ (~3 d). (J) 15 mg ml$^{-1}$, 0.15 mol l$^{-1}$; 0.022 µl h$^{-1}$ (~3 d). Scale bar: 500 µm.

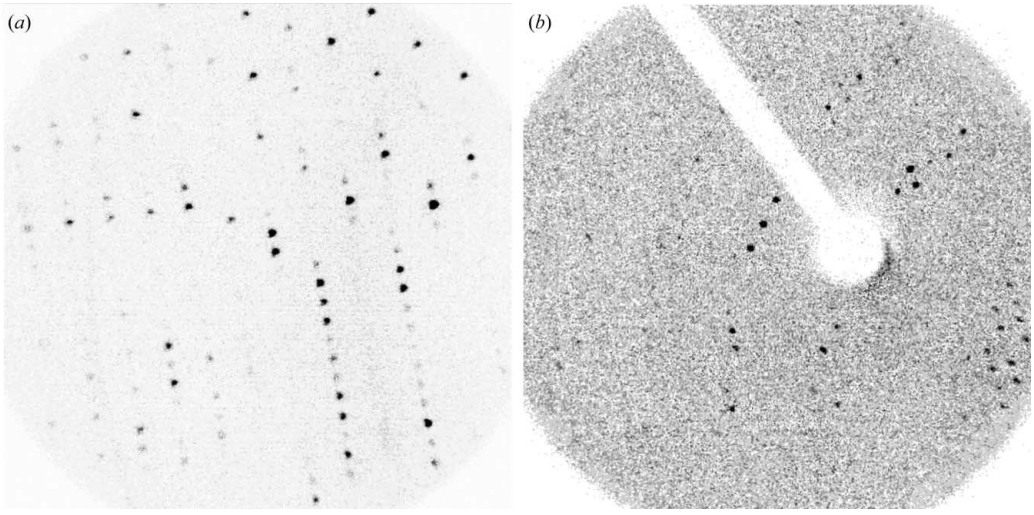


**Figure 4**
X-ray diffraction pattern of crystals of (*a*) lysozyme at 1.5 Å and (*b*) thaumatin at 2.9 Å as obtained with evaporation-based crystallization platforms.

100 g mol$^{-1}$, however, a crystal-producing condition was identified in the most concentrated drop (Fig. 3F; $C_p$ = 15 mg ml$^{-1}$, $C_s$ = 0.15 mol l$^{-1}$). Only small crystals, eventually covered with a film, were observed at lower concentrations (Fig. 3G; $C_p$ = 10 mg ml$^{-1}$, $C_s$ = 0.1 mol l$^{-1}$; and Fig. 3H; $C_p$ = 5 mg ml$^{-1}$, $C_s$ = 0.05 mol l$^{-1}$). These results indicate that for the proteins studied, when starting with drop concentrations below the solubility boundary, higher initial values of $C_p$ result in larger and visually better protein crystals.

### 3.2. Step 2: increasing crystal quality and size

In step 2 for lysozyme, we start from the crystal-producing condition of $C_p$ = 15 mg ml$^{-1}$, $C_s$ = 0.5 mol l$^{-1}$ identified in step 1 (Fig. 3A) and then decrease the evaporation rate from $J$ = 0.42 µl h$^{-1}$ (Fig. 3A), to 0.11 µl h$^{-1}$ (Fig. 3D) and finally to 0.026 µl h$^{-1}$ (Fig. 3E) to yield systematically a few large crystals with minimal visual defects.

The same process is repeated for thaumatin where evaporation is initiated from the crystal-producing condition of $C_p$ = 15 mg ml$^{-1}$, $C_s$ = 0.15 mol l$^{-1}$ identified in Step 1 (Fig. 3F), and the evaporation rate is decreased in nine steps from $J$ = 0.1 µl h$^{-1}$ (Fig. 3F) to 0.022 µl h$^{-1}$ (Fig. 3J). As with lysozyme, a slower rate of evaporation results in fewer and larger crystals when compared with higher evaporation rates.

### 3.3. Confirming crystal quality by X-ray diffraction

To confirm the quality of the crystals obtained with these evaporation-based crystallization platforms, we analyzed them using X-ray diffraction on a Bruker General Area Detector Diffraction System (GADDS), which is equipped with a four-circle diffractometer, a HiStar multiwire area detector, a graphite monochromator and a rotating anode target. A total of 240 frames were recorded using an exposure time of 20 s. Fig. 4 shows the diffraction patterns of crystals of lysozyme (Fig. 4A) and of thaumatin (Fig. 4B) with resolutions of 1.5 Å and 2.9 Å, respectively, which are comparable with literature data (Thorsen *et al.*, 2002; Wiencek, 1999; Juarez-Martinez *et al.*, 2001).

## 4. Discussion

The differences in the precipitation state of the protein can be understood by considering the change in the rate of supersaturation $S$,

$$S(t) = C_p(t)/C_{sat}(t), \tag{2}$$

where $C_p$ is the protein concentration and $C_{sat}$ is the protein concentration at saturation. Note that $C_p$ increases with time because the drop volume is decreasing. $C_{sat}$ decreases with time because the precipitant concentration is also increasing with time. The saturation level $S$ = 1 thus corresponds to the solubility boundary. The concentration $C_i(t)$ of each species '$i$' (protein, precipitants) in the drop at time $t$ can be calculated from

$$C_i(t) = \frac{C_{i0}V_0}{V(t)} = \frac{C_{i0}V_0}{V_0 - Jt} \tag{3}$$

where $C_{i0}$ is the initial concentration of the species $i$, $V_0$ the initial volume, and $V(t)$ the remaining volume at time $t$. Note that $C_{sat}(t)$ is a function of the precipitant identity and concentration ($C_s$), which for lysozyme (Rosenbaum *et al.*, 1996), thaumatin (Juarez-Martinez *et al.*, 2001) and many other proteins is well described by $C_{sat} = \alpha\exp(-\beta[C_s])$, with the parameters $\alpha$ and $\beta$ fitted to solubility data.

Fig. 5 shows supersaturation as a function of time for the three initial conditions for lysozyme of Figs. 3A, 3B and 3C as calculated using equations (2) and (3). Even though a positive driving force for crystal formation exists when $S > 1$, the energy barrier to nucleation at low supersaturation hinders the immediate formation of crystals. This energy barrier decreases as $S$ increases. For lysozyme, the labile region in which crystals nucleate easily was observed for $S > 4$ (McPherson, 1999). Once crystals form, the mass of protein dissolved in the drop decreases and the supersaturation level

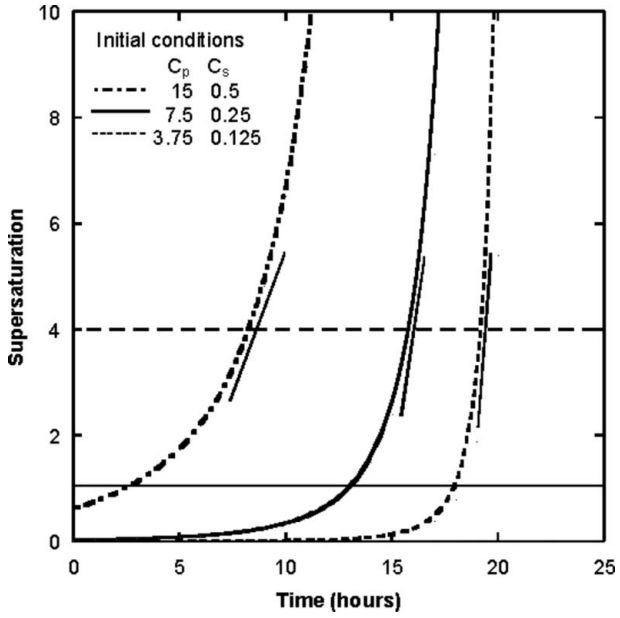


**Figure 5**
Supersaturation as a function of time for the crystallization of lysozyme. The lines are for a 10 µl drop and an evaporation rate $J$ of 0.42 µl h$^{-1}$. These experiments are at different initial conditions but at a constant $C_p/C_s$ ratio of 30 g mol$^{-1}$. The initial conditions correspond to those of the lysozyme experiments in Figs. 3A–3C. The tangential lines indicate the rate of change of supersaturation, while the drop entering the labile region at $S = 4$ (see text) is indicated by the dashed horizontal line. The solid horizontal line at $S = 1$ is the solubility boundary.

in the drop will be significantly lower than that indicated by the curves in Fig. 5.

Three competing processes influence the dissolved protein concentration in the drop. Crystal nucleation and growth both reduce the protein concentration, while evaporation of the solvent increases the protein concentration. If the increase in protein concentration through evaporation is similar to the reduction of the protein concentration caused by crystal formation, the protein concentration in the drop will be nearly constant. However, if the rate of increase in protein concentration due to evaporation is much larger than the rate of decrease by crystal growth, the protein concentration will grow to a point where showers of crystals will rise or a gel boundary is reached. These crystals typically contain defects resulting in poor diffraction patterns (Yoshizaki *et al.*, 2002). The value of $S$ defining the gel boundary will depend on solution conditions but is expected at high protein concentrations and strong strengths of attraction (very low $C_{sat}$) (Kulkarni *et al.*, 2003). Therefore, we hypothesize that if the time to reach the value of $S$ defining the gel boundary is less than what is needed for at least one nucleus to form, the outcome of the experiment will be a gel. Thus we attribute the different outcomes of the lysozyme experiments shown in Figs. 3A (crystals), 3B (few crystals and film) and 3C (film only) to the enhancement of the respective rates of change in supersaturation as indicated by the different slopes at $S = 4$ (typically the metastable-to-labile zone boundary for lysozyme) in Fig. 5.

All three experiments (3A, 3B and 3C) traveled along the same path of constant $C_p/C_s$. To understand the effects of changing rate of supersaturation generation on the state of the protein, we compare the approximate rates by which these different experiments traverse identical sets of conditions along this path. Experiments 3C and 3A each start as a 10 µl drop at 3.75 mg ml$^{-1}$ and 15 mg ml$^{-1}$ of protein, respectively. The drop of experiment 3C needs to lose 7.5 µl to reach the initial condition of experiment 3A. This takes about 15 h at an evaporation rate of 0.5 µl h$^{-1}$. Assuming a critical supersaturation of 4 with the solubility being ~8 mg ml$^{-1}$ (Rosenbaum *et al.*, 1996), each drop will need to reach a protein concentration of ~30 mg ml$^{-1}$ prior to crystal nucleation. This stipulates that the drop of experiment 3A has to lose 5 µl, which takes about 10 h, to reach the protein concentration of ~30 mg ml$^{-1}$. For experiment 3C, only 1.25 µl needs to evaporate to cross the 30 mg ml$^{-1}$ mark, which takes less than 3 h. Thus, lysozyme crystals can nucleate and grow at rates sufficient to keep up with evaporation for rates of increase of protein concentration of ~1.5 mg ml$^{-1}$ h$^{-1}$. A rate of increase of 5 mg ml$^{-1}$ h$^{-1}$ is too high for the nucleation and growth processes to keep up with the loss of solvent and, as a result, films and gels rather than crystals form.

The importance of the rate of change of supersaturation is further apparent in step 2 where we varied $J$ while starting from identical initial conditions. The results for both lysozyme (Figs. 3A, 3D, 3E) and thaumatin (Figs. 3F, 3I, 3J) clearly confirm that the rate of change of supersaturation is critical in producing good quality crystals. Once a crystal-producing condition is identified (Figs. 3A and 3F for lysozyme and thaumatin, respectively), slowing down the rate of change of supersaturation results in larger crystals of high quality suitable for X-ray diffraction.

To demonstrate the advantages of the evaporation-based crystallization method studied here, we have compared its results with results obtained with other crystallization platforms such as HD and MB. Starting with the same arbitrary initial conditions as used in our experiments, only one of the HD experiments produced any crystals and these crystals showed some visual defects (Table 2). None of the MB experiments yielded crystals.

Further validation of our platform is in progress through extensive experimentation with novel proteins. Recently, in collaboration with Yi Lu and coworkers, we were able to grow the crystals of a mutant of cytochrome *c* peroxidase (Ccp) with two redox active tryptophans and six of the tyrosines removed (Pfister *et al.*, 2001). These crystals produced X-ray diffraction patterns with a resolution of 4.6 Å. We are in the process of evaluating the evaporation-based crystallization methodology reported here with more proteins.

## 5. Summary and conclusions

In this paper we report an evaporation-based crystallization platform and protocols for its use to aid in the identification and especially optimization of suitable solution conditions for protein crystallization. In this platform, solvent evaporates

**Table 2**
Comparison of results for different crystallization techniques.

| Initial condition | | | | |
|---|---|---|---|---|
| Protein (mg ml$^{-1}$) | Salt (mol l$^{-1}$) | Microbatch | Hanging drop | Evaporation-based platform |
| Lysozyme in 50 m*M* sodium acetate buffer at pH 4.6 with sodium chloride as the precipitant | | | | |
| 3.75 | 0.125 | No hit | No hit | Film (Fig. 3C) |
| 7.5 | 0.25 | No hit | No hit | Film with few small crystals (Fig. 3B) |
| 15 | 0.50 | No hit | Few crystals; defects and clusters present | Many small crystals (Fig. 3A)<br>Few small crystals (Fig. 3D)<br>Few large crystals (Fig. 3E) |
| Thaumatin in 50 m*M* phosphate buffer at pH 7.0 with sodium potassium tartrate as the precipitant | | | | |
| 5 | 0.05 | No hit | No hit | Showers of small aggregates (Fig. 3H) |
| 10 | 0.10 | No hit | No hit | Showers of small aggregates (Fig. 3G) |
| 15 | 0.15 | No hit | No hit | Many small crystals (Fig. 3F)<br>Fewer small crystals (Fig. 3I)<br>Few large crystals (Fig. 3J) |

from a hanging drop of protein solution in a compartment at a rate that is determined by the dimensions of a channel that connects the compartment to the atmosphere. Unlike current crystallization methods, such as HD, MB and FID, the evaporation-based methodology presented here ensures a phase transition (*i.e.* the formation of gels, precipitates, microcrystals, crystals, *etc.*) in every experiment. Owing to this additional information, fewer experiments are needed in the search for solution conditions that yield high-quality crystals suitable for X-ray diffraction. The platform in its present form is promising in particular for optimization of crystal growth once crystallization conditions are known. Further miniaturization of evaporation-based platforms with multiple compartments and integration of microfluidic networks for automated loading is needed, however, to increase ease of use, to decrease the amount of protein needed per condition screened, and to improve its suitability for initial high-throughput screening of different precipitants. Efforts along these lines are ongoing. Furthermore, implementation of design modifications such as valves in the evaporation channels will enable active control of the rate of change in supersaturation. The latter may be valuable in, for example, reducing the rate of evaporation and thus the rate of crystal growth once a few crystals have nucleated.

The experiments described in this work demonstrate that the quality of the crystal depends on the rate of change in supersaturation. Starting with protein concentrations close to the solubility boundary and using a slow evaporation rate yields high-quality crystals. In addition, the evaporation-based platform enables rapid location of the boundary between the metastable and labile zone, also called the super-solubility curve. The exact time at which crystals are formed can be determined by continuous monitoring of the drop, and since the initial conditions and the rate of evaporation are known, the solution condition (*i.e.* $C_p$ and $C_s$) producing the phase transition that characterizes this metastable to labile boundary can be calculated.

The rate of supersaturation of the protein solution is known to be an important parameter to influence crystal nucleation and growth, and thus quality. Multi-compartment platforms in which each compartment has a different $J$ enable easy screening of a range of supersaturation rates while using droplets with the same initial conditions. Selecting the set of precipitants to be used in the screening experiments remains very much an art based on intuition and past experience as it is for any crystallization protocol. Through the two-step procedure, however, the evaporation-based platform studied here facilitates the evaluation of the appropriateness of each individual precipitant or mixture of precipitants. We envision that further development of heuristic rules that are tailored to different classes of proteins will reduce the number of experiments needed to identify suitable crystallization conditions for proteins. In addition, similar rules can be developed for other molecules, such as DNA, RNA and pharmaceuticals. Furthermore, we will shortly report on the population balance model that provides nucleation and growth kinetic parameters based on experimental data obtained with the crystallization methodology described here.

We thank Venkateswarlu Bhamidi, Gregor Warren and Amit Asthana of our laboratory for help and fruitful discussions. Special thanks are owed to Mr Thomas D. Pfister and Professor Yi Lu for the purification and growth of the Ccp mutant. The diffraction patterns were obtained with the help of Mr Yi-Gui Gao at the 3M Materials Chemistry Laboratory at UIUC. This research was supported by The 3M Corporation, Minneapolis-St. Paul, MN, and the US Department of Energy, Division of Material Science, Grant DEFG02-91ER45439, through the Frederick Seitz Material Research Laboratory at UIUC.

## References

Anderson, V. J. & Lekkerkerker, H. N. W. (2002). *Nature (London)*, **416**, 811–815.
Chayen, N. E. (1997*a*). *J. Appl. Cryst.* **30**, 198–202.
Chayen, N. E. (1997*b*). *Structure*, **5**, 1269–1274.
Collingsworth, P. D., Bray, T. L. & Christopher, G. K. (2000). *J. Cryst. Growth*, **219**, 283–289.
Duffy, D. C., McDonald, J. C., Schueller, O. J. A. & Whitesides, G. M. (1998). *Anal. Chem.* **70**, 4974–4984.
Geankoplis, C. J. (1993). *Transport Processes and Unit Operations*, 3rd ed. New Jersey: Prentice Hall.

Hansen, C. L., Skordalakes, E., Berger, J. M. & Quake, S. R. (2002). *Proc. Natl Acad. Sci. USA*, **99**, 16531–16536.
Hornak, J. P. (1999). *Molecules*, **4**, 353–365.
Juarez-Martinez, G., Garza, C., Castillo, R. & Moreno, A. (2001). *J. Cryst. Growth*, **232**, 119–131.
Kanelis, V., Forman-Kay, J. D. & Kay, L. E. (2001). *Iubmb Life*, **52**, 291–302.
Kulkarni, A. M., Dixit, N. M. & Zukoski, C. F. (2003). *Faraday Discuss.* **123**, 37–50.
McPherson, A. (1999). *Crystallization of Biological Macromolecules*, 1st ed. Cold Spring Harbor Laboratory Press.
Pfister, T. D., Gengenbach, A. J., Syn, S. & Lu, Y. (2001). *Biochemistry*, **40**, 14942–14951.
Rosenbaum, D., Zamora, P. C. & Zukoski, C. F. (1996). *Phys. Rev. Lett.* **76**, 150–153.
Rosenbaum, D. F. & Zukoski, C. F. (1996). *J. Cryst. Growth*, **169**, 752–758.
Sophianopoulos, A. J., Rhodes, C. K., Holcomb, D. N. & Van Holde, K. E. (1962). *J. Biol. Chem.* **237**, 1107–1112.
Thorsen, T., Maerkl, S. J. & Quake, S. R. (2002). *Science*, **298**, 580–584.
Thuman-Commike, P. A. (2001). *FEBS Lett.* **505**, 199–205.
Wiencek, J. M. (1999). *Annu. Rev. Biomed. Eng.* **1**, 505–534.
Yoshizaki, I., Nakamura, H., Sato, T., Igarashi, N., Komatsu, H. & Yoda, S. (2002). *J. Cryst. Growth*, **237**, 295–299.
Zheng, B., Roach, L. S. & Ismagilov, R. F. (2003). *J. Am. Chem. Soc.* **125**, 11170–11171.